Lower Tropospheric Processes; A Control on The Global Mean Precipitation Rate

Jacob Hendrickson[1], Christopher Terai[2], Michael Pritchard[3], and Peter Caldwell[2]

[1]University of California
[2]Lawrence Livermore National Laboratory
[3]University of California Irvine

November 23, 2022

Abstract

The spread in global mean precipitation among climate models is explored in two ensembles using the complementary perspectives of surface evaporation and energy budgets. Models with higher global-mean precipitation have stronger oceanic evaporation, driven by drier near-surface air. The drier surface conditions occur alongside increases in near-surface temperature and moisture at 925 hPa, which point to stronger boundary layer mixing. Correlations suggest that the degree of lower tropospheric mixing explains 18%-49% of the intermodel precipitation variance. To test this hypothesis, the degree of mixing is varied in a single-model experiment by adjusting the relative humidity threshold that controls low-cloud fraction. Indeed, increasing lower tropospheric mixing results in more global mean precipitation. Energetically, increased precipitation rates are associated with more downwelling longwave radiation to the surface and weaker sensible heat fluxes. These results highlight how lower-tropospheric processes must be better constrained to reduce the precipitation discrepancy among climate models.

Lower Tropospheric Processes; A Control on The Global Mean Precipitation Rate

Jacob M. Hendrickson[1], **Christopher R. Terai**[1,2], **Michael S. Pritchard**[1], **Peter Caldwell**[2]

[1]Department of Earth System Science, University of California, Irvine, CA, USA
[2]Lawrence Livermore National Laboratory, Livermore, CA, USA

Key Points:

- CMIP5 AMIP simulations disagree on the magnitude of the present-day global mean precipitation rate by 13%
- Lower tropospheric mixing explains as much as 49% of the inter-model variance
- Up to two-thirds of the atmospheric energy adjustments occur at the surface

Corresponding author: Jacob Hendrickson, `jmhendri@uci.edu`

Abstract

The spread in global mean precipitation among climate models is explored in two ensembles using the complementary perspectives of surface evaporation and energy budgets. Models with higher global-mean precipitation have stronger oceanic evaporation, driven by drier near-surface air. The drier surface conditions occur alongside increases in near-surface temperature and moisture at 925 hPa, which point to stronger boundary layer mixing. Correlations suggest that the degree of lower tropospheric mixing explains 18% - 49% of the intermodel precipitation variance. To test this hypothesis, the degree of mixing is varied in a single-model experiment by adjusting the relative humidity threshold that controls low-cloud fraction. Indeed, increasing lower tropospheric mixing results in more global mean precipitation. Energetically, increased precipitation rates are associated with more downwelling longwave radiation to the surface and weaker sensible heat fluxes. These results highlight how lower-tropospheric processes must be better constrained to reduce the precipitation discrepancy among climate models.

Plain Language Summary

Climate models exhibit a spread in their simulation of the present-day global mean precipitation rate; a fundamental climate statistic whose spread is surprisingly understudied. This 13% spread compares with the expected change in the global mean precipitation rate in a warmer climate scenario. Complex precipitation physics can make understanding what processes control the global mean precipitation rate across climate models inherently difficult. We find that the degree of mixing within the lower 1-km of the atmosphere (lower-tropospheric mixing) controls a large fraction of the spread in global mean precipitation across models. We also show linkages between the lower tropospheric mixing and the energy budget framework that is typically used to understand the global mean precipitation rate. Our results highlight a local scale process (mixing) that controls and impacts a global scale climate statistic (global mean precipitation). They also suggest that future attempts to bridge satellite observations and climate model output can potentially help reduce the existing spread and bias among climate models.

1 Introduction

Global climate models participating in the Fifth Coupled Model Intercomparison Project (CMIP5) differ on the magnitude of the present-day global mean precipitation rate by 13% (orange dots in Fig. S1), a relatively large uncertainty when compared to the 8-12% increase expected from a 4K increase in global temperatures (Deangelis et al., 2015). Reducing this spread would improve confidence in future projections of the water cycle.

Previous studies focusing on the hydrologic cycle's atmospheric energy budget constraint have improved our understanding of how the global mean precipitation may change in a warming climate scenario (e.g. Allen & Ingram, 2002; Stephens & Ellis, 2008; Pendergrass & Hartmann, 2014). Notably, Pendergrass and Hartmann (2014) highlighted the importance of surface, downwelling longwave radiation on future changes of the global mean precipitation. The atmospheric energy budget has also been used to ascertain the flow of energy in the present-day, observed climate (Trenberth et al., 2009; Rodell et al., 2015; Stephens et al., 2012). However, this energetic framework has not, to our knowledge, been applied to understand the large spread in present-day mean precipitation rate among climate models. Meanwhile, we still lack a comprehensive process-oriented theory of what sets the mean state of the global mean precipitation rate. Therefore, our study builds upon past work (e.g. Qian et al., 2015) to better understand what controls present-day, global mean precipitation in climate models.

We intentionally begin our investigation with the analysis of surface water balance to complement an energetic view. In the global average, and on inter-annual or longer timescales, precipitation must equal evaporation. This mass balance allows for global mean precipitation in climate models to be analyzed through a surface evaporation framework (Richter & Xie, 2008; Siler et al., 2019). For example, Waliser and Hogan (2000) noted in their surface flux analysis of a climate model that biases in surface evaporation were partly due to dry air mixing down into the boundary layer over regions where evaporation rates are higher than precipitation rates. This highlights that processes occurring in non-precipitating regions can control the global mean precipitation rate (e.g. Watanabe et al., 2018).

We will show that multi-model ensemble analyses focused on evaporation indicate the importance of lower-tropospheric mixing and that a single-model sensitivity experiment that modifies vertical mixing leads to similar qualitative behavior.

While past work has shown that both the atmospheric energy budget constraint on precipitation and the mechanistic, process-level constraint are both valid, the two views are typically presented separately and reconciling them is difficult. Macro (energetic) and micro (process-oriented) constraints are complementary in the sense that micro-scale processes underlie a macro-scale response. While the energetic framework provides important details about the constraints on global mean precipitation, it does little to offer insight into what processes increase local-scale precipitation or evaporation rates. This has practical implications for attempts to understand how process-scale modeling results, such as those from cloud-resolving simulations, will impact the representation of climate phenomena in global-scale models. Therefore, we focus much of this study on the understudied view of lower-tropospheric mixing on global precipitation rates.

Section 2 of the paper introduces the data sets and our strategy for decomposing latent heat fluxes. Section 3 presents the results and processes found to exert a control on the global mean precipitation rate. We conclude with summary and discussion in Section 4.

2 Data and Methods

To allow a robust sample of present day climate data, we examine two community archives. The first is the well-studied CMIP5 archive (Taylor et al., 2012), comprising monthly output from fifteen simulations spanning 1990 to 2008 (Table S1). In addition to the CMIP5 database, we also examine monthly output from sixteen models archived by the Madden-Julian Oscillation Task Force (MJOTF) model intercomparison; these runs span a comparable time range (1990-2010) (Jiang et al., 2015). We use uncoupled atmosphere-only simulations from both archives, i.e. following the Atmospheric Model Intercomparison Project (AMIP) protocol (Table S1).

To address our goal of investigating why models tend to disagree on the magnitude of the present-day global mean precipitation rate, we begin by sorting the models within both the CMIP5 and MJOTF ensembles by their global-mean precipitation rates and forming composite anomalies from the five rainiest minus five driest ensemble members.

A "bottom-up" analysis of mean precipitation differences is prohibitively complicated since precipitation is produced by many interacting parameterization schemes, the number and nature of which differ from model to model. To sidestep these issues we exploit the balance in the atmospheric water budget on annual to interannual timescales. That is, global mean precipitation must equal global mean evaporation. Focusing on present-day global mean evaporation controls, we look at how different model components and representation of physical processes affect latent heat fluxes via the bulk formula (Fairall et al., 1996) as

$$H_L = \rho L_v C_e V_1 (q_0 - q_1), \tag{1}$$

where H_L, is the turbulent flux of latent heat, ρ is the density of air, L_v is the latent heat of vaporization (assumed to equal $2.501 * 10^6\, J\, kg^{-1}$), C_e is the transfer coefficient for latent heat fluxes, V_1 is the near-surface 10-meter horizontal wind speed, q_0 is the saturation specific humidity based on sea surface temperatures, and q_1 is the 2-m specific humidity.

3 Results

3.1 CMIP5 and MJOTF

To investigate the model spread in global mean precipitation we examine which variable exerts a significant control on model spread in evaporation rates, eventually implicating the near-surface specific humidity q_1 as especially interesting. Other factors are less obviously important. For instance, the density of air (ρ) varies insignificantly from model to model, and hence does not provide insight into the model spread. One reason we use AMIP rather than ocean-coupled simulations is because it conveniently controls for the term q_0: the saturation specific humidity based on the sea surface temperatures of the model cannot vary due to common boundary conditions. The bulk transfer coefficient of water vapor, C_e, is inherently difficult to disentangle due to its dependence on a number of factors including stability and momentum roughness, both of which depend on the surface fluxes themselves (Neale et al., 2012). Thus, the bulk transfer coefficient is not investigated in this analysis.

This leaves two variables to investigate, wind speed and low level humidity. Although the near surface wind speed V_1 is known to have a significant impact on local evaporation, a preliminary analysis suggests that intermodel variations in wind speed are only weakly correlated to the global mean evaporation rate (Fig. S2). Thus, we are left to investigate q_1; the near surface specific humidity.

It is logical to expect a drier surface would support more evaporation, and indeed we find this to be the case in composite anomaly maps (Fig S3). However, a drier surface and more evaporation alone do not provide insight into what controls surface humidity. Is the entire atmospheric column drier in the rainier models? Or are regional effects of horizontal advection or lower tropospheric vertical mixing the cause of spread in local surface humidity? Such questions motivate unfolding vertical structures, and in Figure 1a-c we examine the composite differences of specific humidity profiles at three locations over the tropical ocean; a deep convection region (SPCZ), a region of trade cumulus clouds and an area of persistent stratocumulus clouds in the eastern Pacific Ocean.

Notably, models that rain more have a consistent departure from the mean vertical structure compared to those that rain less (Fig. 1a-c). In models that rain more, the 1000 hPa humidity tends to be lower. However, there also exists a layer of elevated moisture levels around 950 to 850 hPa. Not only is this canonical vertical anomaly structure consistent across different regions, it is also seen in both the CMIP5 and MJOTF datasets.

Our working hypothesis is that the association between a drier surface and more moisture near the top of the boundary layer implies varying levels of lower tropospheric mixing, which brings down dry and warm (potential temperature) air to the surface while replenishing it aloft. This leads to drier surface air and more evaporation. Consistent with this hypothesis, we find near-surface air temperature to not be only drier but also warmer in the models that precipitate more (Fig. S4).

To summarize so far, we speculate that in the models that rain more lower tropospheric mixing is stronger. The stronger lower tropospheric mixing weakens the verti-

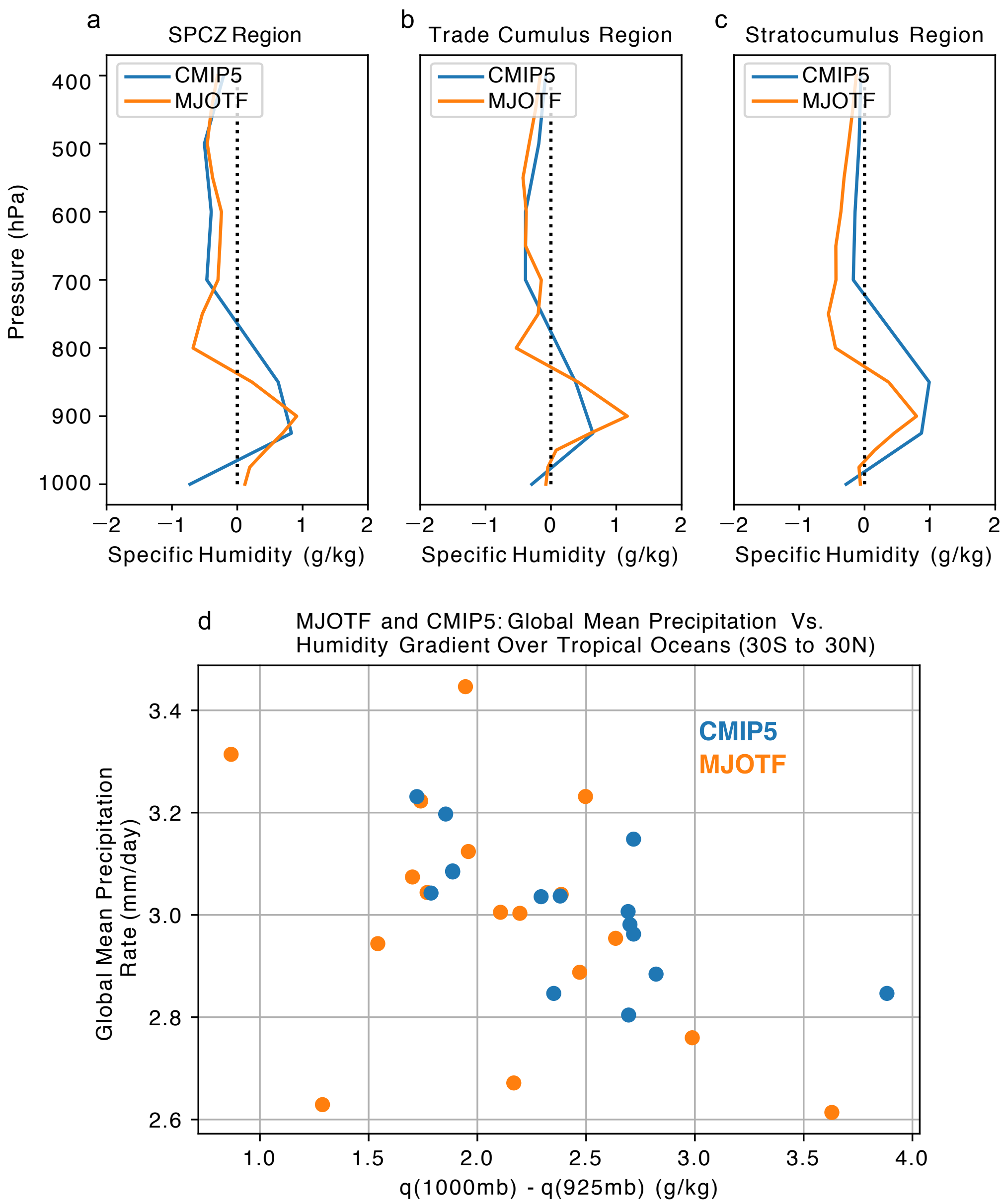

Figure 1 (a-c) Time averaged specific humidity anomalies at 3 locations from climate models participating in the MJO Task Force intercomparison (MJOTF - orange) and in the Atmospheric Model Intercomparison Project of CMIP5 (CMIP5 - blue). Anomalies represent differences between the 5 rainiest and 5 driest models in each ensemble. (d) The specific humidity difference between 1000hPa and 925hPa, averaged over tropical oceans is plotted against the global mean precipitation rates. Each CMIP5 model is indicated by a blue dot while the MJOTF models are displayed as orange dots.

cal moisture gradient within the boundary layer and produces anomalous warming and drying of the near-surface air. These physical responses then lead to more evaporation and because what evaporates must eventually precipitate; the end result is a larger amount of precipitation in the global mean.

Inspired by the vertical structure of the humidity anomaly in Fig. 1a-c, we use the difference between 1000 hPa and 925 hPa humidity as our proxy for mixing. The composite anomaly maps of this proxy confirm robustness across large fractions of multiple tropical ocean basins (Fig. S5). There have been several other metrics that have indirectly captured lower tropospheric mixing in the context of cloud feedbacks and equilibrium climate sensitivity (e.g. Sherwood et al., 2014; Brient et al., 2016). The advantage of this study's proxy is its simplicity, its availability across most models, and direct connection with mixing. Furthermore, where the models overlap, we have confirmed our metric strongly correlates with the specific humidity diffusivity as reported by Brient et al. (2016).

Lower tropospheric mixing is certainly not the only physical mechanism leading to the large spread in present-day global mean precipitation rates across climate model simulations. However, it explains a significant amount of the variance - as much as 18% (49%) of the inter-model variance in precipitation across the MJOTF (CMIP5) datasets is explained by our humidity gradient proxy metric averaged over the tropical oceans (Fig. 1d).

3.2 A sensitivity test to vary boundary layer mixing in the Community Atmosphere Model Version 5.0

A note on causal ambiguity is appropriate since diagnostics alone are not sufficient to fully confirm the hypothesis that lower tropospheric mixing is behind the spread. Thus, we perform a sensitivity test aimed at exploring causality. Our strategy is to modulate low-cloud fraction in the Community Atmosphere Model Version 5.0 (Neale et al., 2012). The reasoning is threefold. First, our mixing proxy suggest model spread associated with lower tropopsheric mixing is especially strong in regions of stratocumulus clouds (Fig. S5). Second, in those regions, radiative cooling at stratocumulus cloud top significantly drives lower atmospheric overturning (Wood, 2012). Third, low clouds have been found to be quite important to climate changes in precipitation from the complementary viewpoint of column atmospheric energetics (Watanabe et al., 2018), thus allowing the sensitivity test to be useful from both the surface-evaporation (mixing) and the radiative (energetic) conceptual framework.

We proceed by targeting a parameter of the Park-Bretherton cloud-fraction parameterization scheme, RH_{minl}, which sets the relative humidity threshold for the formation of low-level clouds (Park & Bretherton, 2009). Some prominent effects on the global mean precipitation rate have already been linked to this parameter in a perturbed physics ensemble experiment by Qian et al. (2015). Does varying RH_{minl} produce the same vertical humidity structures that we have argued are indicative of vertical mixing in the CMIP5 and MJOTF model ensemble?

To find out, five CAM5 model configurations are run for three years, each with a different RH_{minl} ranging from 81% to 96.5%. The lowest threshold corresponds to a larger cloud fraction and a larger magnitude of lower tropospheric mixing (Fig. 2).

We then create composite anomalies to investigate the structure of humidity within the lowest part of the atmosphere, analogous to what was shown for multi-model intercomparison in Fig. 1a-c. These profiles confirm a familiar vertical structure as seen in the analysis of the multi-model ensembles. The signal is weaker than in the CMIP5 and MJOTF datasets (see Table S2), but the hallmark of the sensitivity test is that a similar vertical dipole in lower tropospheric moisture occurs across the interference experiments, which are consistent with more mixing in the lower troposphere (Fig. 2c). Global mean precipitation also responds in the direction expected from a leading control by surface humidity via the evaporation framework (Table S2). Thus, using the same metric to quantify lower tropospheric mixing, we find that the CAM5 experiment provides some confirmation that tuning the lower tropospheric mixing, even if indirectly, can affect the global mean precipitation rate.

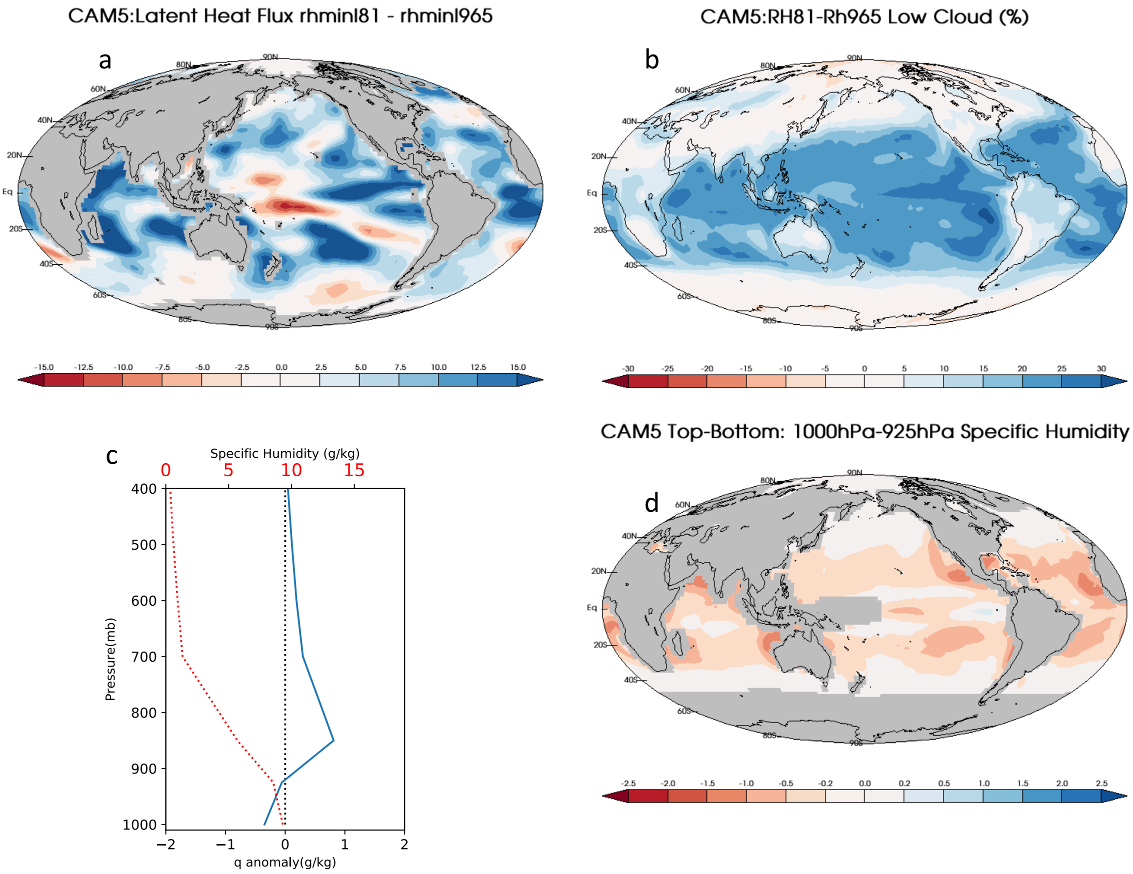

Figure 2 (a) Map of evaporation difference between the simulations with lowest threshold for the formation of low clouds (rhminl81) and the highest threshold for the formation of low clouds (rhminl965). (b) Map of the low cloud difference between rhminl81 and rhminl965. (c) Time averaged mean state specific humidity (red line) and anomaly between rhminl81 and rhminl965 (blue line) over a region of persistent stratocumulus clouds. (d) Map of the specific humidity gradient difference (lower tropospheric mixing metric), quantified as the humidity difference between 1000hPa and 925hPa, between the rhminl81 and the rhminl965 simulations.

3.3 Viewing the sensitivity experiment from the energetic lens

We now switch conceptual frameworks from the surface evaporation lens, which emphasizes an important role for vertical mixing in modifying global mean precipitation, to consider the complementary view of column atmospheric energetics, in which radiative effects can become very important.

Conservation of energy requires that an increase in latent heat flux due to increased global mean precipitation must be balanced by other energetic fluxes out of or into the atmosphere (e.g. Stephens & Ellis, 2008; Pendergrass & Hartmann, 2014) . Mathematically,

$$\frac{dE}{dt} = R_{SW} - R_{LW} + L + S, \tag{2}$$

where dE/dt is the atmospheric energy storage rate, R_{SW} is net atmospheric absorption of shortwave radiation, R_{LW} is net atmospheric emission of longwave radiation,

L is the latent heat flux, and S is sensible heat flux. On annual or longer timescales, we can assume little to no storage of energy in the atmosphere and thus

$$L = R_{LW} - R_{SW} - S. \tag{3}$$

Using Eq. 3, we can investigate which terms balance the latent heat flux when we modify lower-tropospheric mixing by changing the amount of low clouds within the CAM5 experiments.

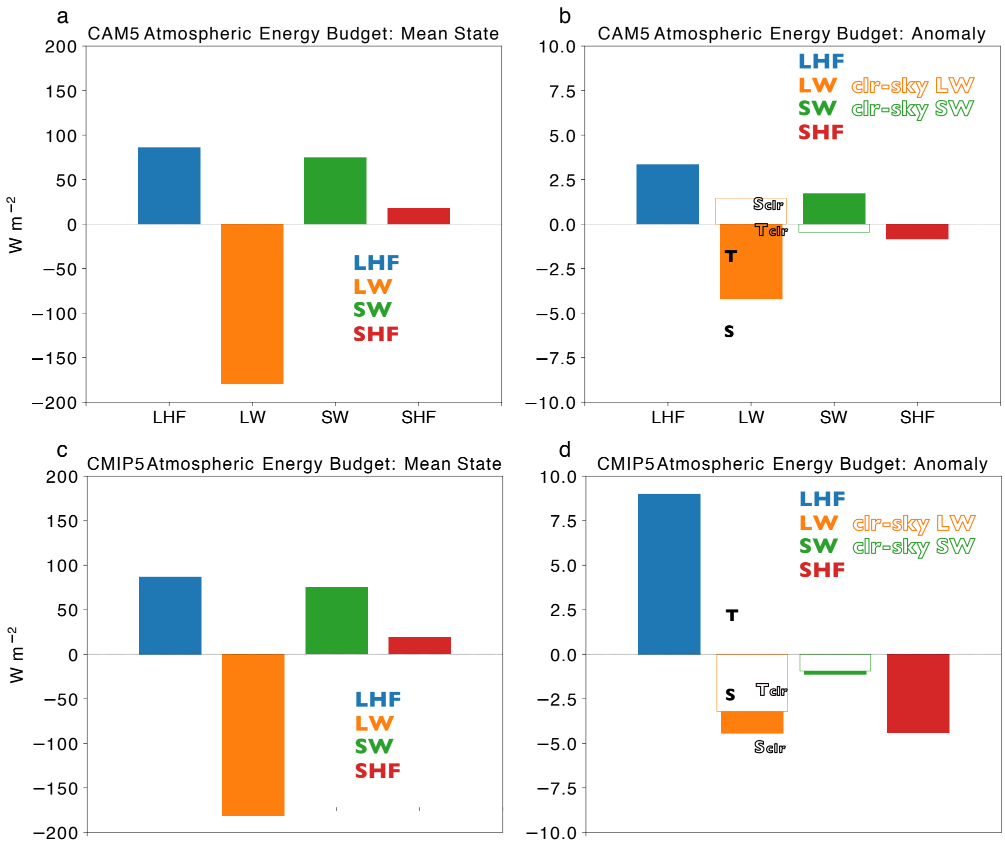

Figure 3 Atmospheric energy budget means and anomalies for the CAM5 experiments and CMIP5 ensemble. a) CAM5 mean atmospheric energy budget. Each bar represents mean latent heat flux (blue), all-sky longwave flux (orange), all-sky shortwave flux (green), and sensible heat flux (red) into the atmosphere. b) Corresponding anomalies between the CAM5 model experiments with the highest and lowest global mean precipitation rate. Orange and green edged bars indicate clear-sky anomalies for longwave and shortwave anomalies. Anomalies of all-sky and clear-sky top-of-atmosphere longwave fluxes (T and T_{clr}) and all-sky and clear-sky surface longwave flux anomalies (S and S_{clr}) are also shown. c) Same as a) but corresponding to CMIP5 ensemble means. d) Same as b), but with anomalies between the 5 most-raining models and 5 least-raining models from the CMIP5 ensemble.

In the mean, longwave cooling is largely balanced by latent and sensible heat fluxes (Fig 3a). When the threshold for low-cloud formation is lowered and low-cloud fraction increases, this leads to greater latent heat flux, which is compensated by stronger longwave cooling out of the atmosphere (Fig 3b). Based on the conventional view of longwave cooling compensating increased latent heat fluxes, we might expect longwave fluxes to have increased at the top-of-atmosphere, but in the CAM5 experiments, this is not the case. Instead, the decrease in net longwave flux at the surface explains the increased longwave cooling, mostly caused by an increased longwave flux downward in cloudy conditions (Fig 3b). In hindsight, this strong control of surface longwave fluxes makes sense - removing low-lying clouds does not have a major longwave effect at TOA due to little contrast between the cloud top temperature and the sea surface temperature, but does have a major effect at the surface due to changes in emissivity affecting downwelling longwave radiation (Wood, 2012).

Pendergrass and Hartmann (2014) found in a warming climate scenario that increased lower tropospheric water vapor concentrations leads to increased downward longwave radiative fluxes to compensate the increase in global-mean latent heat fluxes. Somewhat consistent with this, we find that differences in latent heat flux in the CAM5 experiments are compensated by changes that occur in the lower-troposphere, rather than in the upper troposphere, albeit they are for cloudy scenes.

In summary, the change in low-cloud cover from adjusting RH_{minl} increases longwave cooling at the top of the boundary layer. This drives increased turbulent mixing of warm dry air to the surface to enhance latent heat fluxes but also increases downwelling longwave radiation. This is analogous to the finding by Watanabe et al. (2018) who found in global warming experiments that models with a stronger decrease in low clouds exhibited a weaker increase in evaporation with warming.

3.4 Viewing the CMIP5 experiments from the energetic lens

We again use Eq. 3, but this time for the CMIP5 simulations, and examine whether, as for the vertical mixing signatures, there is consistency between the CAM5 experiments test and the multi-model analysis from the energetic lens. As in the CAM5 experiments (Sect. 3.3), the CMIP5 model ensemble also shows that most (two-thirds) of the energetic adjustments occur at the surface (Fig. 3d). A third of the energetic adjustment is due to increased longwave cooling at the top of atmosphere. Unlike the CAM5 experiments, however, the surface longwave differences are mainly from clear-sky radiative differences. The longwave adjustment also only explains half of the excess latent heat flux. The other half is explained by a decrease in sensible heat flux. This importance of the sensible heat flux in balancing latent heat flux is consistent with previous results that highlight how variations in sensible heat flux explain the trends in global mean precipitation in historical simulations (Myhre et al., 2018).

We now ask, what conditions are likely behind a decrease in sensible heat flux and an increase in downward surface longwave radiative fluxes in clear-sky conditions? In the global warming context, Pendergrass and Hartmann (2014) have noted that an increase in near-surface humidity due to a warming explains the increasing downward surface longwave flux in the global warming context. In our case, previous analysis (Fig 1a-c) shows that in models that rain more in the present-day climate, the near-surface is actually drier, but also warmer.

If we further ask why the near-surface air temperature is warmer, we arrive at two possible explanations. First, the whole temperature profile might be warmer in models that rain more. Such a condition can happen just from stronger latent heating in the atmosphere. Second, the surface air temperature might be warmer due to vertical gradients in the temperature that allow a warmer surface air. This second explanation is closely tied to the vertical mixing in the lower-troposphere, for stronger vertical mixing will drive air with higher potential temperature down to the surface. Figure S4 provides some clues to their relative importance. In the CMIP5 models, the potential temperature of the air column is higher by approximately 0.5 K in models that rain more (Fig. S4). However, the surface air temperature difference is consistently higher than the rest of the column. Without this difference in the vertical structure, the energetic adjustments would be weaker.

In summary, the previous two sections provide the energetic view of what controls the global mean precipitation. In both our CAM5 experiments and CMIP5 ensemble, it is the surface energetic fluxes that mainly determine how the excess latent heating is balanced. In the CAM5 experiments, the increased downward surface longwave flux is a direct result of the parameter that was used to change the amount of vertical mixing. In the CMIP5 ensemble, two-thirds of the adjustments are in the sensible heat flux and the clear-sky, downward, longwave radiative fluxes at the surface. Their cause is likely a warmer surface air temperature, part of which is due to a warmer air column but part of which is due to a warmer surface air temperature compared to the rest of the column. This contribution of the lower tropospheric stability to the energetic adjustments and its connection to lower tropospheric mixing provides a glimmer of how we might reconcile a mechanstic and energetic approach to understanding the global mean precipitation rate.

4 Discussion and Conclusion

The spread in global mean precipitation across climate models is a longstanding issue. Even in modern climate model simulations, there exists a 13% spread in present-day global mean precipitation rates. Analyzing this spread through an evaporation framework provides some insight into what local-scale mechanisms help produce the spread in the global mean precipitation. A metric was constructed to quantify the portion of intermodel spread in global mean precipitation rates that can be linked to lower tropospheric mixing. This is quantified by the specific humidity gradient between 1000hPa and 925hPa and can be characterized by bringing down dry and warm air (Fig. 1a-c and Fig. S4). We find that models that rain more tend to have stronger lower tropospheric mixing. This leads to a warmer and drier surface and subsequently more evaporation. Simple linear regressions across each of the CMIP5 and MJOTF ensembles indicate that lower tropospheric mixing explain 18% and 49% of the inter-model variance in global mean precipitation rates, respectively.

As a test of cause and effect, we run a model experiment with the CAM5 global climate model by tuning a parameter that controls the relative humidity threshold for low cloud formation. This tuning in turn modulates the rate of lower tropospheric mixing, because stratocumulus clouds are not only driven by, but also drive, the subcloud turbulence that sustains them, providing a strong lever on lower tropospheric mixing that is conveniently co-located with geographic action centers that are especially prominent in model spread. In our single-model experiment, we find that the model with more global mean precipitation rate exhibits same vertical structures in humidity found in CMIP5 and MJOTF, namely a drier surface and moister layer right above. Thus, we can say with some confidence that disagreements between models on the global mean precipitation rate can be partially explained by lower tropospheric mixing.

This model experiment raises the possibility of a feedback between precipitation and lower tropospheric mixing, where greater global mean precipitation rates increases tropospheric mixing through changes in low-cloud cover. Increased latent heating in the middle troposphere over the convective regions typically increases tropospheric stability, which by itself will not increase mixing. The increased stability, however, might increase low-cloud cover, driving more lower tropospheric mixing. One can speculate whether this is occurring in the CMIP5 and MJOTF ensembles. Two points suggest that it is not. First, a look at the potential temperature differences in Fig. S3 does not indicate more lower-tropospheric stability between 700 hPa and 1000 hPa over the trade cumulus and stratocumulus regions. Second, a cross-model correlation between the global mean precipitation rate and local cloud fractions below 680 hPa in the CMIP5 ensemble do not show a strong positive correlation over the tropical oceans (not shown).

Acknowledging that an energetic framework also provides insight into the reasons behind the inter-model spread in global mean precipitation rate, we examine which of the surface and top-of-atmosphere energetic fluxes balance the difference in latent heat flux. In both the CAM5 experiments and CMIP5 ensemble, the energetic adjustments mainly occur at the surface and the downward, longwave flux at the surface plays a substantial role. Because the relative humidity threshold for low-cloud cover was changed when we modulated the lower-tropospheric mixing in the CAM5 experiments, decreasing the threshold, which increased global mean precipitation rates, also increased low-cloud cover and increased the downward, surface longwave fluxes. In contrast, the energy flux adjustments in the CMIP5 ensemble do not involve cloud-radiative changes. Instead, the increased latent heat flux is mainly balanced by a stronger clear-sky, downward, longwave radiative fluxes at the surface and a weaker sensible heat flux. Both are consistent with a warmer surface air temperature, and hence with increased lower-tropospheric mixing. Note that the energetic framework is complementary to the mechanistic approach that we have taken in this study and the fact that we can explain the precipitation rate using one framework does not negate or diminish the importance of understanding the other framework. A full understanding of the spread in the global mean precipitation rate requires understanding the reasons for the spread using both frameworks.

Given their importance to the mean-state climate, our result highlights how future attempts to constrain climate sensitivity of global mean precipitation can benefit from including arguments about lower tropospheric mixing. Much progress has been made in the attempt to explicitly resolve boundary layer and cloud processes (Pressel et al., 2014; Schneider et al., 2017; Parishani et al., 2018) at the global scale but it is still computationally cumbersome at long timescales. Furthermore, the higher precipitation rates in climate models, when compared to observational estimates (e.g. Terai et al., 2018), suggest that climate models might be overestimating lower tropospheric mixing. These are at odds with a recent study of Hourdin et al. (2015), which conclude that in coupled model simulations, a persistent warm bias in sea surface temperatures is likely due to models not mixing enough in the lower troposphere. It brings attention to the much needed observations to validate lower-tropospheric turbulent processes in next-generation climate models.

We can speculate on the use of instruments and methods that provide highly resolved, in both time and space, boundary layer measurements of moisture and temperature. As an indirect method of measuring lower tropospheric mixing, active lidar or passive microwave sensors could be deployed to measure low-level moisture fields. Great promise in obtaining continuous moisture and temperature profiles, which provide a way of measuring instability and fluxes of temperature and moisture in the boundary layer, have been made in recent years (e.g. Froidevaux et al., 2013). Beyond the speculation of a deploying lidar and radar sensors across the global oceans, we can make use of observational data already available to the scientific community (e.g. NASA's Atmospheric Infrared Sounder retrievals - AIRS). AIRS does not provide a direct method of measuring turbulent fluxes but has proved useful as a measure of stability in the lower troposphere (e.g. Yue et al., 2011).

Our analysis provides insight into local scale processes that impact global scale evaporation and thus, precipitation within the confines of climate simulations. However, more work is needed to be done to bridge the gap between models and observational data that is readily available, highlighting the need to identify whether current observations are adequate in coverage, resolution, and accuracy to constrain local-scale processes, which have impacts on global-scale climate statistics.

Acknowledgments

Jacob Hendrickson and Christopher Terai are supported by NASA grant 80NSSC18K0756; Mike Pritchard acknowledges additional support from NSF grants AGS-1734164 and AGS-

191213. Peter Caldwell was supported by the Energy Exascale Earth System Model (E3SM) project, funded by the U.S. Department of Energy, Office of Science, Office of Biological and Environmental Research. A portion of this work was conducted under the auspices of the U.S. Department of Energy by Lawrence Livermore National Laboratory under Contract DE-AC52-07NA27344. IM-Release: LLNL-JRNL-812658-DRAFT

We thank Xianan Jiang for providing us access to the MJOTF datasets. The U.S. Department of Energy's (DOE) Program for Climate Model Diagnosis and Intercomparison provides coordinating support and led development of software infrastructure for CMIP5 in partnership with the Global Organization for Earth System Science Portals. The model output was downloaded from and can be obtained from the Earth System Grid Federation at https://esgf-node.llnl.gov/projects/cmip5/.

References

Allen, M. R., & Ingram, W. J. (2002). Constraints on future changes in climate and the hydrologic cycle. *Nature*, *419*(6903). doi: 10.1038/nature01092

Brient, F., Schneider, T., Tan, Z., Bony, S., Qu, X., & Hall, A. (2016, 7). Shallowness of tropical low clouds as a predictor of climate models' response to warming. *Climate Dynamics*, *47*(1-2), 433–449. doi: 10.1007/s00382-015-2846-0

Deangelis, A. M., Qu, X., Zelinka, M. D., & Hall, A. (2015). An observational radiative constraint on hydrologic cycle intensification. *Nature*, *528*(7581), 249–253. Retrieved from `http://dx.doi.org/10.1038/nature15770` doi: 10.1038/nature15770

Fairall, C. W., Bradley, E. F., Rogers, D. P., Edson, J. B., & Young, G. S. (1996). Fairall_et_al-1996-Journal_of_Geophysical_Research__Solid_Earth_(1978-2012). , *101*, 3747–3764.

Froidevaux, M., Higgins, C. W., Simeonov, V., Ristori, P., Pardyjak, E., Serikov, I., … Parlange, M. B. (2013). A Raman lidar to measure water vapor in the atmospheric boundary layer. *Advances in Water Resources*, *51*, 345–356. Retrieved from `http://dx.doi.org/10.1016/j.advwatres.2012.04.008` doi: 10.1016/j.advwatres.2012.04.008

Hourdin, F., Ginus-Bogdan, A., Braconnot, P., Dufresne, J. L., Traore, A. K., & Rio, C. (2015). Air moisture control on ocean surface temperature, hidden key to the warm bias enigma. *Geophysical Research Letters*, *42*(24), 10885–10893. doi: 10.1002/2015GL066764

Jiang, X., Waliser, D. E., Xavier, P. K., Petch, J., Klingaman, N. P., Woolnough, S. J., … Zhu, H. (2015). Vertical structure and physical processes of the madden-julian oscillation: Exploring key model physics in climate simulations. *Journal of Geophysical Research*, *120*(10), 4718–4748. doi: 10.1002/2014JD022375

Myhre, G., Samset, B. H., Hodnebrog, O., Andrews, T., Boucher, O., Faluvegi, G., … Voulgarakis, A. (2018). Sensible heat has significantly affected the global hydrological cycle over the historical period. *Nature Communications*, *9*(1). Retrieved from `http://dx.doi.org/10.1038/s41467-018-04307-4` doi: 10.1038/s41467-018-04307-4

Neale, R. B., Gettelman, A., Park, S., Chen, C.-c., Lauritzen, P. H., Williamson, D. L., … Taylor, M. a. (2012). Description of the NCAR Community Atmosphere Model (CAM 5.0). NCAR Technical Notes. *Ncar/Tn-464+Str*.

Parishani, H., Pritchard, M. S., Bretherton, C. S., Terai, C. R., Wyant, M. C., Khairoutdinov, M., & Singh, B. (2018). Insensitivity of the Cloud Response to Surface Warming Under Radical Changes to Boundary Layer Turbulence and Cloud Microphysics: Results From the Ultraparameterized CAM. *Journal of Advances in Modeling Earth Systems*, *10*(12), 3139–3158. doi: 10.1029/2018MS001409

Park, S., & Bretherton, C. S. (2009). The University of Washington shallow convection and moist turbulence schemes and their impact on climate simulations with the community atmosphere model. *Journal of Climate*, *22*(12), 3449–3469. doi: 10.1175/2008JCLI2557.1

Pendergrass, A. G., & Hartmann, D. L. (2014). The atmospheric energy constraint on global-mean precipitation change. *Journal of Climate*, *27*(2), 757–768. doi: 10.1175/JCLI-D-13-00163.1

Pressel, K. G., Mishra, S., Schneider, T., Kaul, C. M., & Tan, Z. (2014). Journal of Advances in Modeling Earth Systems. *Journal of Advances in Modeling Earth Systems*, *6*, 1065–1094. doi: 10.1002/2014MS000363.Received

Qian, Y., Yan, H., Hou, Z., Johannesson, G., Klein, S., Lucas, D., ... Zhao, C. (2015). Parametric sensitivity analysis of precipitation at global and local scales in the Community Atmosphere Model CAM5. *Journal of Advances in Modeling Earth Systems*, *7*(2), 382–411. doi: 10.1002/2014MS000354

Richter, I., & Xie, S. P. (2008). Muted precipitation increase in global warming simulations: A surface evaporation perspective. *Journal of Geophysical Research Atmospheres*, *113*(24), 1–20. doi: 10.1029/2008JD010561

Rodell, M., Beaudoing, H. K., L'Ecuyer, T. S., Olson, W. S., Famiglietti, J. S., Houser, P. R., ... Wood, E. F. (2015). The observed state of the water cycle in the early twenty-first century. *Journal of Climate*, *28*(21), 8289–8318. doi: 10.1175/JCLI-D-14-00555.1

Schneider, T., Teixeira, J., Bretherton, C. S., Brient, F., Pressel, K. G., Schär, C., & Siebesma, A. P. (2017). Climate goals and computing the future of clouds. *Nature Climate Change*, *7*(1), 3–5. Retrieved from `http://dx.doi.org/10.1038/nclimate3190` doi: 10.1038/nclimate3190

Sherwood, S. C., Bony, S., & Dufresne, J. L. (2014). Spread in model climate sensitivity traced to atmospheric convective mixing. *Nature*, *505*(7481), 37–42. doi: 10.1038/nature12829

Siler, N., Roe, G. H., Armour, K. C., & Feldl, N. (2019). Revisiting the surface-energy-flux perspective on the sensitivity of global precipitation to climate change. *Climate Dynamics*, *52*(7-8), 3983–3995. Retrieved from `http://dx.doi.org/10.1007/s00382-018-4359-0` doi: 10.1007/s00382-018-4359-0

Stephens, G. L., & Ellis, T. D. (2008). Controls of global-mean precipitation increases in global warming GCM experiments. *Journal of Climate*, *21*(23), 6141–6155. doi: 10.1175/2008JCLI2144.1

Stephens, G. L., Li, J., Wild, M., Clayson, C. A., Loeb, N., Kato, S., ... Andrews, T. (2012, 10). An update on Earth's energy balance in light of the latest global observations. *Nature Geoscience*, *5*(10), 691–696. doi: 10.1038/ngeo1580

Taylor, K. E., Stouffer, R. J., & Meehl, G. A. (2012, 4). *An overview of CMIP5 and the experiment design* (Vol. 93) (No. 4). doi: 10.1175/BAMS-D-11-00094.1

Terai, C. R., Caldwell, P. M., Klein, S. A., Tang, Q., & Branstetter, M. L. (2018). The atmospheric hydrologic cycle in the ACME v0.3 model. *Climate Dynamics*, *50*(9-10), 3251–3279. doi: 10.1007/s00382-017-3803-x

Trenberth, K. E., Fasullo, J. T., & Kiehl, J. (2009). Earth's global energy budget. *Bulletin of the American Meteorological Society*, *90*(3), 311–323. doi: 10.1175/2008BAMS2634.1

Waliser, D. E., & Hogan, T. F. (2000, 2). Analysis of ocean surface heat fluxes in a NOGAPS climate simulation: Influences from convection, clouds and dynamical processes. *Journal of Geophysical Research Atmospheres*, *105*(D4), 4587–4606. doi: 10.1029/1999JD901028

Watanabe, M., Kamae, Y., Shiogama, H., DeAngelis, A. M., & Suzuki, K. (2018, 10). Low clouds link equilibrium climate sensitivity to hydrological sensitivity. *Nature Climate Change*, *8*(10), 901–906. doi: 10.1038/s41558-018-0272-0

Wood, R. (2012). Stratocumulus clouds. *Monthly Weather Review*, *140*(8), 2373–2423. doi: 10.1175/MWR-D-11-00121.1

Yue, Q., Kahn, B. H., Fetzer, E. J., & Teixeira, J. (2011). Relationship between marine boundary layer clouds and lower tropospheric stability observed by AIRS, CloudSat, and CALIOP. *Journal of Geophysical Research Atmospheres*, *116*(18). doi: 10.1029/2011JD016136

Geophysical Research Letters

Supporting Information for

Lower Tropospheric Processes; A Control on The Global Mean Precipitation Rate

Jacob M. Hendrickson[1], Christopher R. Terai[1], Michael S. Pritchard[1], Peter Caldwell[2]

1. Department of Earth System Science, University of California, Irvine, CA, USA 2. Lawrence Livermore National Laboratory, Livermore, CA, USA

Contents of this file

Figures S1 to S6
Tables S1 to S2

Introduction

This document contains the supplemental figures referenced in the main manuscript

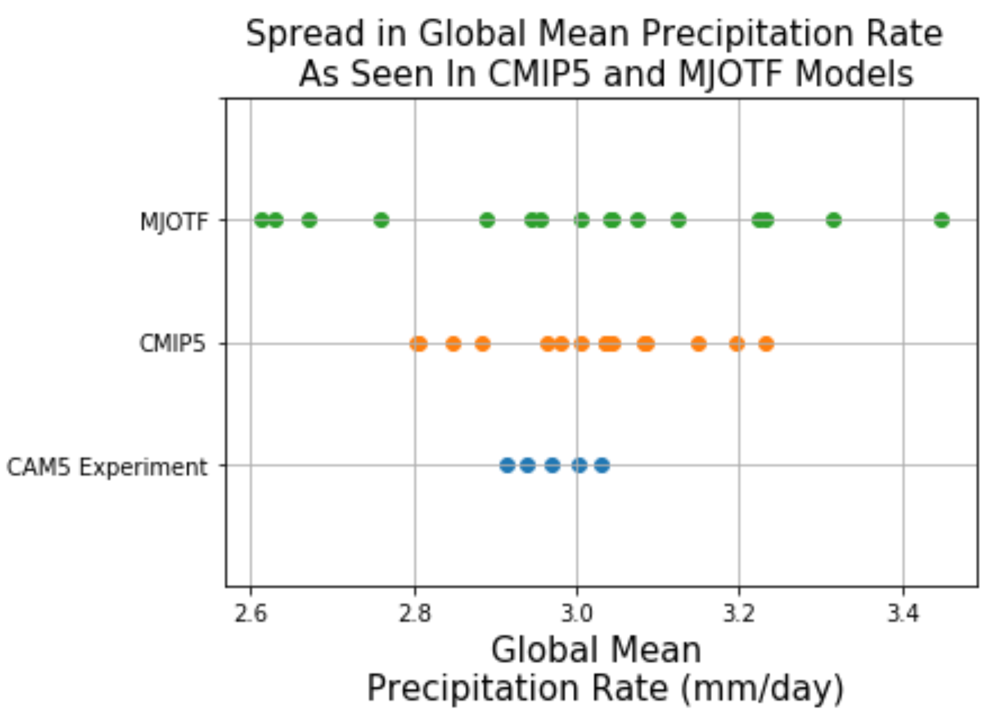

Figure S1. *The global mean precipitation rate from atmosphere-only climate model simulations participating in the MJO Task Force intercomparison (MJOTF - green), the Atmospheric Model Intercomparison Project of CMIP5 (CMIP5 - orange), and from five configurations of the CAM5 model where the threshold relative humidity for stratiform low clouds (rhminl) is perturbed (blue).*

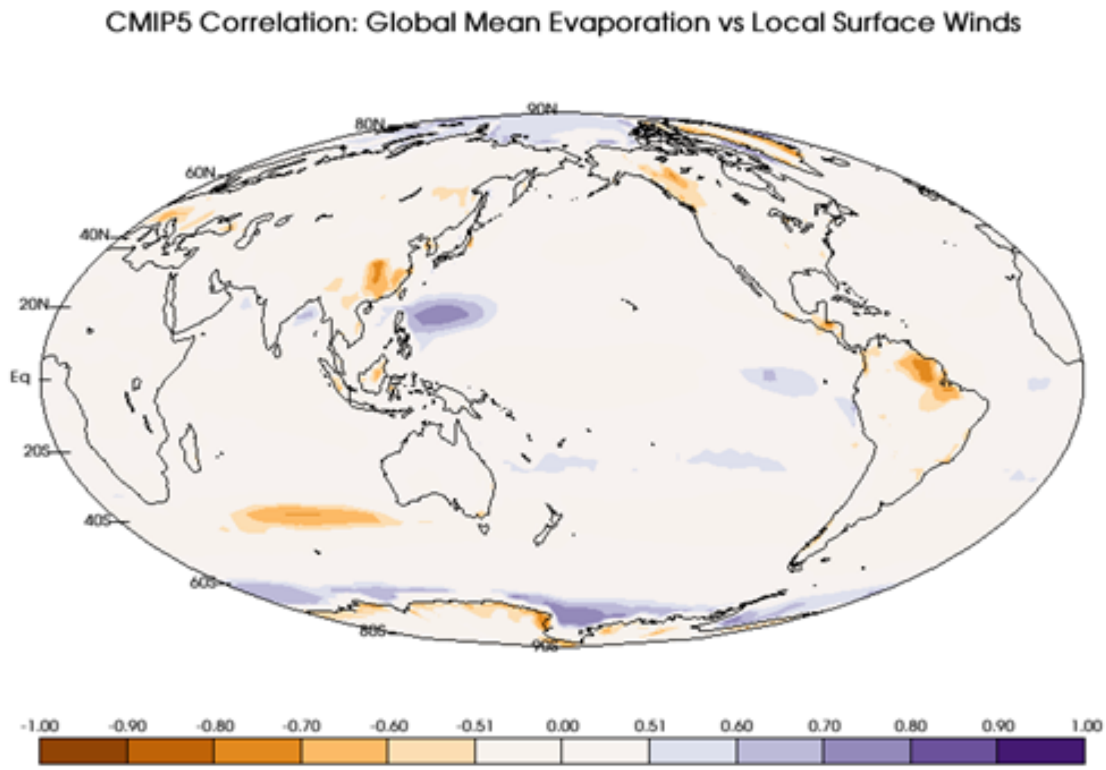

Figure S2. *Correlation map of the global mean precipitation rate from climate models participating in the Atmospheric Model Intercomparison Project of CMIP5 vs time averaged near surface winds. Correlations with magnitudes below 0.51 are in gray because they are not significant at the 95\% level for a sample size of fifteen.*

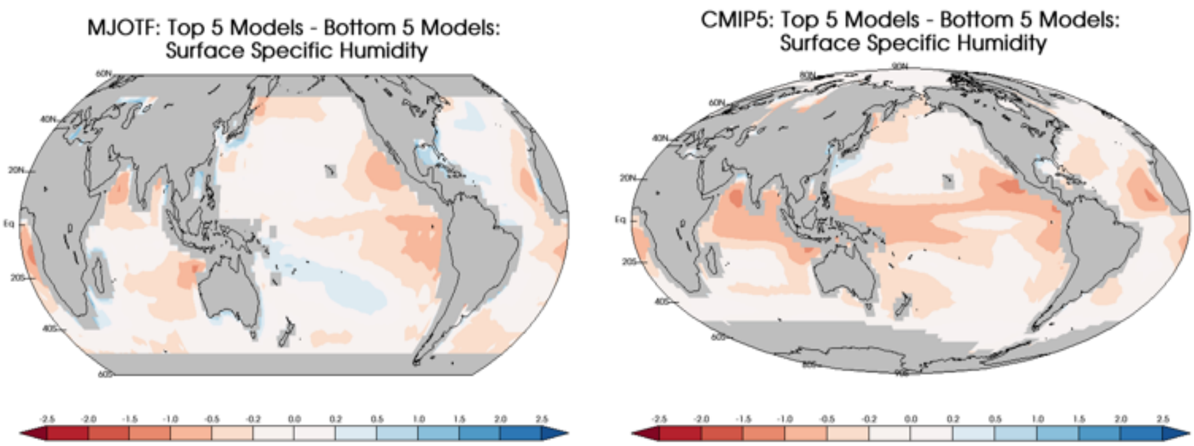

Figure S3. *Time averaged surface specific humidity anomalies derived from climate models participating in the MJO Task Force intercomparison (MJOTF - left) spanning 1991 to 2010, and from climate models participating in the Atmospheric Model Intercomparison Project of CMIP5 (CMIP5 - right) spanning 1991 to 2005*

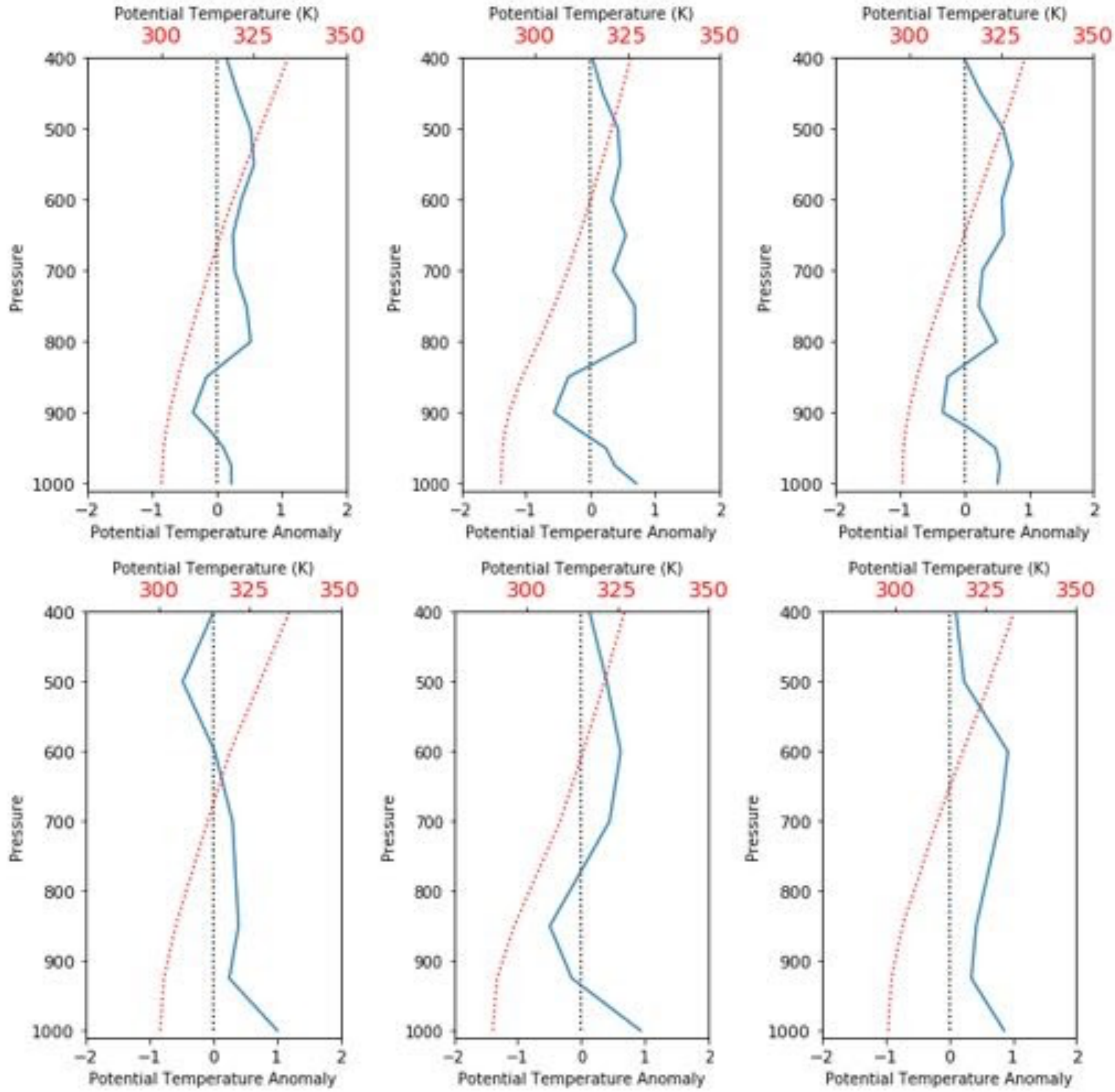

Figure S4. *Time averaged potential temperature anomalies over the SPCZ, a region of persistent stratocumulus clouds and a region characterized by trade cumulus clouds (oriented from left to right). They are derived from climate models participating in the MJO Task Force intercomparison (MJOTF - top) spanning 1991 to 2010, and from climate models participating in the Atmospheric Model Intercomparison Project of CMIP5 (CMIP5 - Bottom) spanning 1991 to 2005.*

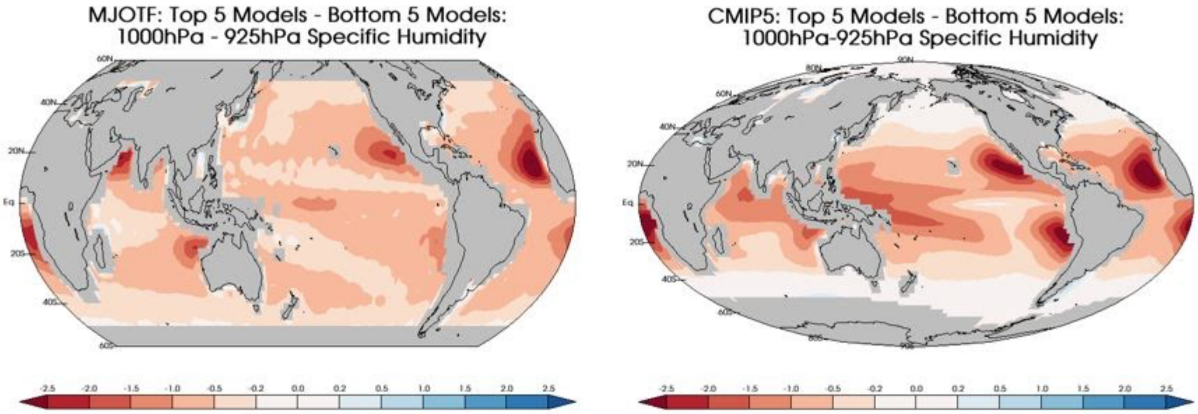

Figure S5. *Time averaged anomalies of the lower tropospheric mixing metric, defined as the specific humidity gradient between 1000hPa and 925hPa, derived from climate models participating in the MJO Task Force intercomparison (MJOTF - left) spanning 1991 to 2010, and from climate models participating in the Atmospheric Model Intercomparison Project of CMIP5 (CMIP5 - right) spanning 1991 to 2005.*

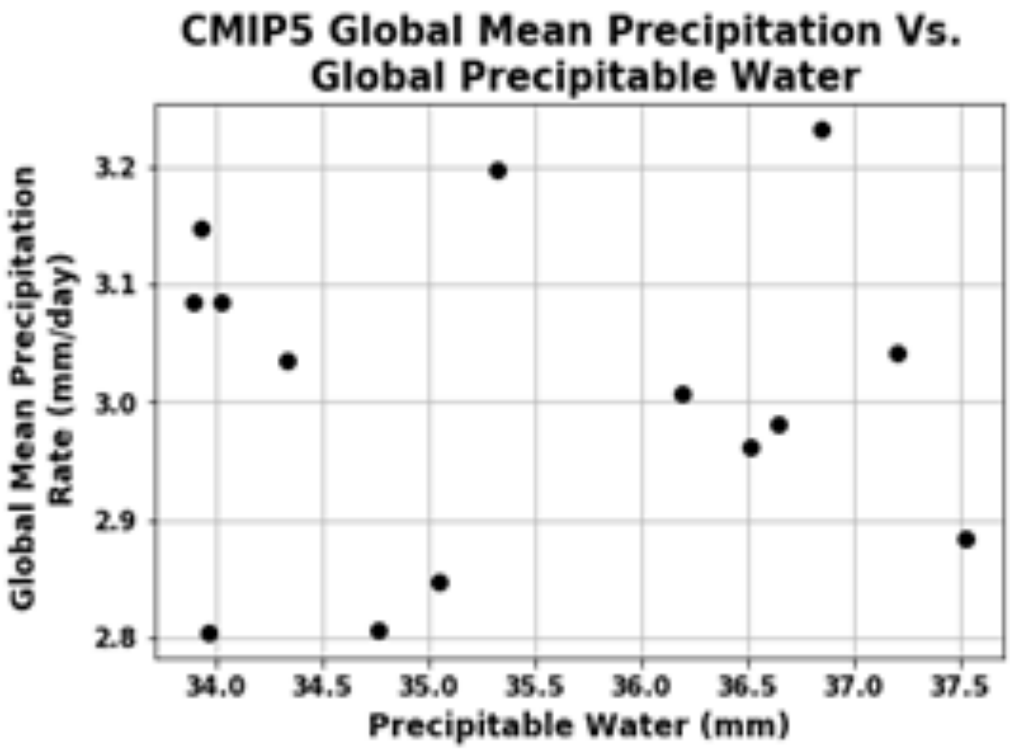

Figure S6. *The global mean precipitation rate from climate models participating in the Atmospheric Model Intercomparison Project of CMIP5 plotted against global precipitable water. A consistent ocean mask is used across the MJOTF and CMIP5 models to compute these averages.*

CMIP5	GMP/ σ $(mm\ d^{-1})$	MJOTF	GMP/ σ
Miroc5	3.23	CWB-GFS	3.45
ACCESS1-3	3.20	GISS-E2	3.31
GISS-E2-R	3.15	MIROC5	3.22
ACCESS1-0	3.09	NCEPCPC-CFS2	3.23
Hadgem2-A	3.08	MetUM-GA3	3.12
Top 5 Multi-Model Mean	3.15	**Top 5 Multi-Model Mean**	3.27
Top 5 Model σ	0.06	**Top 5 Model σ**	0.11
IPSL-CM5A-LR	2.81	NavGEM1	2.61
CanAM4	2.80	ECGEM	2.63
IPSL-CM5B-LR	2.85	BCC-AGCM2.1	2.67
NORESM1-M	2.88	FGOALS-s2	2.76
CCSM4	2.96	ISUGCM	2.89
Bottom 5 Multi-Model Mean	2.86	**Bottom 5 Multi-Model Mean**	2.71
Bottom 5 Model σ	0.06	**Bottom 5 Model σ**	0.10
CESM1-CAM5	3.04	GMAO_GEOS5	2.94
CNRM-CM5	3.04	MRI-AGCM	3.01
GFDL-CM3	3.04	NCAR-CAM5	3.04
MPI-ESM-LR	2.98	CNRM-AM	3.04
MPI-ESM-MR	3.01	LLNL-CAM5	3.07
		SMHI-ecearth3	2.95

Table S1.: *Global mean precipitation rate (GMP), 5 model mean and 5 model standard deviation from the top 5 and bottom 5 CMIP5(left column) and MJOTF(right Column) AMIP ensemble members. The rest of the ensemble members, from each ensemble, are also listed below the bottom 5 model standard deviation.*

CAM5 Model Experiment			
Model Configuration	**RH Threshold for the Formation of Low-Clouds**	**GMP$(mm\ d^{-1})$**	**Δq Averaged over Tropical Oceans $(g\ kg^{-1})$**
Rhmin81	81%	3.03	1.74
Rhmin85	85%	3.00	1.83
Rhmin8875	88.75%	2.97	1.92
Rhmin925	92.5%	2.94	2.06
Rhmin965	96.5%	2.91	2.15

Table S2. *Five CAM5 model experiment configurations, relative humidity thresholds for the formation of low-level clouds(rhminl), global mean precipitation rate and the lower tropospheric mixing metric (Δq) averaged over tropical oceans.*